



HAL
open science

Transient landscape dynamics across the Southeastern Australian Escarpment

Vincent Godard, Anthony Dosseto, Jules Fleury, Olivier Bellier, Lionel Siame,
Team Aster

► **To cite this version:**

Vincent Godard, Anthony Dosseto, Jules Fleury, Olivier Bellier, Lionel Siame, et al.. Transient landscape dynamics across the Southeastern Australian Escarpment. *Earth and Planetary Science Letters*, 2019, 506, pp.397-406. 10.1016/j.epsl.2018.11.017 . hal-02085967

HAL Id: hal-02085967

<https://amu.hal.science/hal-02085967>

Submitted on 1 Apr 2019

HAL is a multi-disciplinary open access archive for the deposit and dissemination of scientific research documents, whether they are published or not. The documents may come from teaching and research institutions in France or abroad, or from public or private research centers.

L'archive ouverte pluridisciplinaire **HAL**, est destinée au dépôt et à la diffusion de documents scientifiques de niveau recherche, publiés ou non, émanant des établissements d'enseignement et de recherche français ou étrangers, des laboratoires publics ou privés.

Transient landscape dynamics across the Southeastern Australian Escarpment

Vincent Godard^{a,*}, Anthony Dosseto^b, Jules Fleury^a, Olivier Bellier^a, Lionel Siame^a, ASTER Team^{a,1}

^a*Aix Marseille Univ, CNRS, IRD, INRA, Coll France, CEREGE, Aix-en-Provence, France*

^b*Wollongong Isotope Geochronology Laboratory, School of Earth and Environmental Sciences, University of Wollongong, Australia*

Abstract

Passive margin escarpments provide some of the best examples for large-scale transient landscape evolution. Despite the relative simplicity of their geological setting, when compared with active orogenic systems, many open questions exist concerning their modes and rates of evolution. We use catchment wide denudation rates calculated from cosmogenic nuclides concentrations and high resolution topographic analysis to constrain landscape dynamics across the South Eastern Australian Escarpment. We determined denudation rates of ~ 15 mm/ka in the lowlands at the foot of the escarpment and of ~ 10 mm/ka in the highlands, while catchment draining the escarpment face display rates in the 20-60 mm/ka range. These denudation rates along a passive margin escarpment are among the highest in the world and show greater sensitivity to topographic gradients when compared to other passive margin settings. We interpret this situation as resulting from the intermediate precipitation regime of our study area, as opposed to drier or wetter settings, where hillslope processes can be inhibited due to water availability or deep weathering profiles and vegetation feedbacks, respectively. Combined with the extraction of topographic metrics across the escarpment, these rates allow us to constrain efficiency coefficients for fluvial incision and hillslope diffusion that are similar to other independent estimates in this region. These coef-

*Corresponding author

Email address: godard@cerege.fr (Vincent Godard)

¹Georges Aumaître, Didier L. Bourlès, Karim Keddadouche

ficients are used to calculate an escarpment retreat rate of 40 to 80 mm/ka over the last 100s of ka. Our analysis of high resolution hillslope morphological properties suggests widespread small-scale disequilibrium across this landscape, illustrating the pervasiveness of transience across all spatial scales in this geomorphological setting.

Keywords: Landscape Evolution, Cosmogenic Nuclides, Denudation, Transient dynamics, Continental Escarpment, High resolution satellite imagery

1. Introduction

Landscapes evolves through time under the competing influences of internal (tectonics) and external (climate) forcings, which drive weathering, erosion and sediment transport processes. Most theoretical formulations of surface processes suggest that landscapes and sediment fluxes can achieve a state of equilibrium where these forcings equilibrate each other. Nevertheless, evidence for transient evolution is widespread in natural landscapes and is characterized by temporal changes in various properties, such as elevation, planar organization, denudation and sediment fluxes, away from idealized steady state structures and behaviors (e.g. Mudd, 2017). Such unsteadiness can be observed across all the range of spatial scales, from the response of a single hillslope profile (e.g. Hurst et al., 2013), to the reorganization of drainage divides over several tens of kilometers (e.g. Beeson et al., 2017). Similarly, the corresponding timescales encompass the whole spectrum from the dramatic changes in river transport due to a single storm event, to the continual adjustment of landscapes to background tectonic and climatic boundary conditions over millions of years. It is also noteworthy that transient adjustments of landscapes have been observed across diverse tectonic boundary conditions from rapidly uplifting active orogenic systems (e.g. Fox et al., 2014) to much more stable cratonic domains (e.g. Czarnota et al., 2014). The study of transience has also been of primary importance in geomorphology, because the examination of transient responses may provide information on erosion laws and their controlling parameters that are not directly available from steady state solutions (e.g. Tucker and Whipple, 2002). Due to the diversity of the processes involved and their wide range of response timescales, these observations question whether steady-state is a common situation in natural landscapes. Investigation of landscape dynamics

usually focus on a particular length scale of interest for the characterization of transient evolution. However, robust evidence exists for the coexistence of both steady state and transient regimes inside a landscape, depending on the wavelength of the considered geomorphic processes or features (e.g. Heimsath et al., 2000). Characterizing the various manifestations of transience across spatial scales appears to be a critical element for our understanding of landscape evolution processes.

Among the diversity of geomorphological systems allowing the study of transient landscape evolution, passive margin escarpments stand out as some of the most propitious. It can be noted that, (1) they are one of the most salient features of continental relief outside of orogenic areas, with major topographic steps (>1000 m) separating high-standing plateaus from lowland coastal plains, (2) their long wavelength history is intrinsically defined by the migration of the escarpment step away from the coast and (3) the absence of major tectonic forcing leads to an evolution dominated by surface processes. Despite the apparent relative simplicity of their structure and dynamics when compared with active mountain ranges, numerous first-order questions, connected to their transient dynamics, remain open.

These questions include, for example, whether the escarpment evolves by self-parallel retreat of its edge or by downwearing of the plateau located seaward from a pre-existing inland drainage divide (e.g. figure 1 from Braun and van der Beek, 2004). The rates of the processes governing the long-wavelength evolution have also been highly discussed, with proposed velocities for escarpment retreat spanning several orders of magnitude from 10 m/Ma to 1 km/Ma (e.g. Weissel and Seidl, 1997; Cockburn et al., 2000; Braun, 2018). Diverse approaches have been used to quantify the rates of escarpment evolution and test the proposed models : geological and geomorphological analysis at different length-scales (e.g. Nott et al., 1996; Weissel and Seidl, 1997; Matmon et al., 2002; van der Beek and Braun, 1998), low-temperature thermochronology to document the exhumation patterns over 10-100 Ma timescales (e.g. Persano et al., 2002; Braun and van der Beek, 2004), as well as denudation rates deduced from cosmogenic nuclides on shorter timescales (e.g. Cockburn et al., 2000; Heimsath et al., 2006; Salgado et al., 2014). The dynamics of passive margins escarpments have also been extensively scrutinized using numerical Surface Processes Models (Braun, 2018, and references therein). However, among these numerous studies, very few have investigated in details the relationship between denudation rates and high resolution morphological properties across the escarpment, an approach

that has provided important insights into the transient dynamics of other types of landscapes (e.g. Hurst et al., 2012, 2013). Furthermore, even if the transient nature of these escarpments dynamics has already been extensively illustrated, most studies have focused on its long-wavelength expression at the regional scale or along river profiles, and the manifestations of transience across various spatial scales, down to individual hillslopes, remain poorly constrained. Additionally, the occurrence of steady state at some spatial scales is an important assumption required by some of the methods used in many studies cited above.

Here, the combination of high resolution topographic data with denudation rates derived from cosmogenic nuclides is used to characterize the recent dynamics of the South Eastern Australian Escarpment (SEAE). The datasets acquired in this study allow us to constrain the erosion efficiency coefficients for fluvial and hillslope processes in order to derive estimates of the retreat rate of the escarpment (Braun, 2018), but also to compare hillslopes morphological parameters with steady-state predictions in order to assess the transient dynamics of various landscape elements from the escarpment foot to the highland plateau.

2. Setting

We focus our study on the Bega catchment, near the southern end of the SEAE (Figure 1). This area is dominated by granitoid bedrock and presents a simple general configuration where the drainage divide is located close to the escarpment edge. The Bega catchment has been at the center of numerous previous geological, geochronological and geomorphological studies (e.g. Heimsath et al., 2001; Persano et al., 2002; Braun and van der Beek, 2004; Green et al., 2006), providing a dense background allowing to carry out further investigations of the escarpment landscape dynamics.

The Bega river drains the eastern flank of the Great Dividing Range that marks the SEAE. The escarpment is assumed to have been created during the Cretaceous rifting of the Tasman Sea, 80-100 Ma ago. Many evolution models advocate for a rapid initial stage of lateral propagation of the escarpment from its initial position after rifting, followed by a period of significantly slower evolution (e.g. Persano et al., 2002). Contrasting rates of escarpment retreat have been reported along the South-Eastern Australia coast. For example, based on low-temperature thermochronology data, Persano et al. (2002) argue for recent stability and low retreat rates of the escarpment near

the Bega valley, which is consistent with finding from other escarpments worldwide using other methodologies (e.g. Cockburn et al., 2000; Matmon et al., 2002). On the other hand, ~ 700 km farther north along the escarpment, Weissel and Seidl (1997) reported retreat rates of the order of 1 km/Ma. Additional data are needed to further discuss this difference in rates, but it could be related to the way landscape average denudation is converted into horizontal divide mobility (Braun, 2018).

The SEAE is currently located ~ 50 km inland in our study area, the continental divide being directly at or close to the escarpment edge (Figure 1). The eastern lowlands areas draining to the sea globally lie at 100-400 m a.s.l., whereas the highlands draining into the Murray-Darling river system have an elevation around 1000 m a.s.l.. The landscape of the Bega catchment is dominated by gently rolling hillslopes with low landsliding activity (e.g. Heimsath et al., 2001, 2006) up to the escarpment edge, which displays higher slopes and dissection than the surrounding areas (Figure S1). Farther west, the highland plateau is characterized by lower relief than the escarpment area. The bedrock geology is dominated by the granitoids of Silurian and Ordovician ages from the Bega Batholith in most of the Bega catchment, with widespread occurrences of Cenozoic basalts in upland areas. Studies aiming at understanding soil production and transport in the wider frame of the escarpment evolution have been performed in the Bega valley and the surrounding areas (e.g. Heimsath et al., 2006; Green et al., 2006; Heimsath et al., 2010; Dosseto et al., 2008). Several studies allowed not only to document the rate of soil production and support the exponential shape of the soil production function (Heimsath et al., 2000, 2001), but also helped constraining the mode of soil transport (Heimsath et al., 2002) or the nature and timing of the weathering processes (e.g. Dosseto et al., 2014).

3. Methods

In this study we combined two methodological approaches to assess the geomorphological evolution across the South Eastern Australian Escarpment (SEAE) at 10-100 ka timescales. Firstly, we use cosmogenic nuclides (^{10}Be) concentration measurements in river sediments to derive catchment-wide denudation rates (CWDR). Secondly, Pléiades satellite imagery is used to produce high-resolution Digital Elevation Models (DEM). Pléiades satellites acquire panchromatic multi-stereo views of a scene during the same orbit with a resolution of 0.5 m. They provide a cost-effective alternative to airborne

LiDAR in settings without dense forest cover and where vegetation is dominated by grass. Couples of images were processed using standard photogrammetric techniques in order to extract high resolution DEM (1 m pixel size) across the escarpment and document topographic properties at the hillslope scale (Figure 2). Details of the analytical procedures, methods and datasets are presented in the Supplementary Materials.

The combination of the two types of data used here, describing both landscape morphology and rates of evolution is based on hillslope dynamics formulations presented in earlier studies (Roering et al., 2007; Hurst et al., 2012; Grieve et al., 2016). Hillslope sediment flux q_s has been proposed to be primarily controlled by topographic gradients S , either linearly as $q_s = K_d S$ or non-linearly as $q_s = K_d S / (1 - (S/S_c)^2)$, where K_d is a sediment transport efficiency coefficient and S_c a critical hillslope gradient. Combining these transport laws with a statement for sediment conservation allows to derive an expression for hillslope profile evolution, and in particular to relate morphological properties measured from high resolution topographic data such as slope or curvature, with rates of evolution, such as surface denudation $\dot{\epsilon}$ calculated from cosmogenic nuclides concentrations. For example, in low relief areas where the sediment flux can be considered to be a linear function of topographic gradient, steady state hillslope elevation z varies with horizontal coordinate x as,

$$z(x) = \frac{\beta \dot{\epsilon}}{2K_d} (x^2 - L_H^2), \quad (1)$$

where β is the rock to regolith density ratio and L_H the hillslope length. The hillslope total relief R can then be expressed as,

$$R = \frac{\beta \dot{\epsilon} L_H^2}{2K_d}, \quad (2)$$

which yields a linear relationship between average hillslope gradient \bar{S} and denudation rate :

$$\bar{S} = \frac{\beta \dot{\epsilon} L_H}{2K_d}. \quad (3)$$

When topographic gradients are low, as it the case near hilltops in most of our study area, a direct relationship exist between hilltop curvature C_{HT} , $\dot{\epsilon}$ and K_d (e.g. Hurst et al., 2012),

$$C_{HT} = \frac{\beta \dot{\epsilon}}{K_d}. \quad (4)$$

We can define $R_R = S_c L_H$ a reference relief corresponding to the maximum relief for a hillslope of length L_H , and $E_R = K_d S_c / (2\beta L_H)$ a reference erosion rate (Roering et al., 2007). The critical slope S_c is introduced in these definitions for compatibility with non-linear formulations. Dividing equation 2 by S_c provides,

$$\frac{R}{S_c L_H} = \frac{R}{R_R} = \frac{\beta \dot{\epsilon} L_H}{2K_d S_c} = \frac{\dot{\epsilon}}{4E_R}, \quad (5)$$

which can be cast as a relationship between non dimensional relief R^* and erosion rate E^* in the case of an equilibrium hillslope,

$$R^* = \frac{1}{4} E^* \quad (6)$$

A more complex relationship can be derived between R^* and E^* in the case of a non-linear sediment flux (Roering et al., 2007). Using equation 4 the non-dimensional erosion rate can be directly calculated from measurable topographic parameters as $E^* = 2C_{HT} L_H / S_c$.

4. Results

Concentrations measured in the 18 sampled basins range from 100 to 874×10^3 at/g (average and standard deviation : $257 \pm 216 \times 10^3$ at/g, Table S1) which lead to CWDR ranging from 59 to 8 mm/ka (average and standard deviation : 25 ± 13 mm/ka). The average CWDR calculated from samples draining exclusively the lowlands is 16 ± 1 mm/ka (Figure 3). Samples from the highlands lead to an averaged denudation rate of 13 ± 6 mm/ka, or 10 ± 3 mm/ka when excluding the outlying sample BG28, which is similar to rates reported by Portenga et al. (2016) in the highlands farther north and by Heimsath et al. (2001) in an adjacent catchment. Catchments draining the high-slope areas of the escarpment edge display rates ranging from 18 to 59 mm/ka (average 32 ± 13 mm/ka), consistent with CWDR reported by Heimsath et al. (2000, 2006) for the Nunnock river (Fig. 1). The obtained CWDR are positively and significantly correlated with catchment-averaged topographic metrics and proxies for the intensity of hillslopes denudation or fluvial incision, such as average topographic gradient and normalized steepness index calculated from ASTER GDEM 30 m resolution Digital Elevation Model (Figure 4 and supplementary materials). We note that two catchments (BG25 and BG26) stand out of the general trends. These two catchments encompass the headwaters of the Bega river, where water diversion occurs

near the base of the escarpment due a power plant installation. Sediments originating from the upper part of these catchments are therefore lacking in the samples we collected. Both catchments are thus not considered in the following analysis.

The processing of Pléiades-derived high resolution DEM allowed us to extract hilltop curvature as well as hillslope length and relief along a profile through the escarpment. One of the most striking features of this morphometric analysis is the low variability of the investigated parameters in the lowland area, at the foot of the escarpment. Hilltop curvature is $0.0068 \pm 0.0030 \text{ m}^{-1}$, whereas hillslope length and relief are 104 ± 37 and 16 ± 7 m, respectively. In the highland plateau, curvature is $0.0042 \pm 0.0028 \text{ m}^{-1}$, which is consistent with the lower denudation rates characterizing this area (Hurst et al., 2012). Hillslope relief at 13 ± 11 m is similar to the lowland section, whereas hillslope length slightly increases to 126 ± 66 m, which implies a decrease in the average hillslope angle and is again consistent with lower CWDR in the highlands.

5. Discussion

We first discuss the denudation rate dataset presented here in the general frame of landscape evolution across escarpments considered globally. We note that the absence of pronounced tectonic forcing along passive margin escarpments offers a great opportunity to focus directly on the influence of climate on surface processes. Then, we use the temporal constraints on landscape evolution we obtained from our CWDR and the high-resolution spatial characterization of landscape morphological properties obtained from our DEM, to discuss the transient dynamics of the area from the scale of the escarpment to that of the hillslope.

5.1. Denudation processes across the escarpment

Our study document a full Catchment-Wide Denudation Rate (CWDR) transect across a passive margin escarpment using cosmogenic nuclides (Figure 3), which allows to obtain a long-wavelength perspective on surface processes operating across such a major topographic feature over 10 to 100 ka timescales according to the integration time of our CWDR. As shown in the presentation of the results, denudation rates obtained in the Bega region are in line with previous estimates along this escarpment, both in the Highlands (Portenga et al., 2016) and in the escarpment face (Heimsath et al., 2001). Both denudation, weathering and soil evolution processes have already been

extensively documented in the Bega valley. Punctual measurements of surface denudation highlights significant differences between soil lowering rates and bedrock denudation, which testify for small scale instabilities and transient adjustments operating across the landscape, even though steady state denudation is also locally achieved at some sites (Heimsath et al., 2000). At longer wavelengths, the 3 to 4-fold difference between denudation rates calculated in basins draining across the escarpment and the highlands is also an indication of transience and suggests active retreat processes at work toward the hinterland.

When compared with data from various passive margin escarpment settings, it is noteworthy that, for a given range of hillslope angles, the denudation rates in the Bega area appear to be significantly higher than those determined in similar geological contexts (Figure 5A), such as the Serra do mar in Brazil (Salgado et al., 2014; Cherem et al., 2012), the Western Ghats of India (Mandal et al., 2015) or the South African escarpment (Scharf et al., 2013). The significantly lower denudation rates reported in South Africa have been attributed to a major lithological control on denudation, due to the occurrence of widespread resistant quartzite bedrock. It has also been recognized that the low denudation rates observed in Sri Lanka, despite high mean annual precipitation, resulted from the development of thick alteration profiles in this hot and wet environment, that shield the bedrock from the direct action of weathering agents (von Blanckenburg et al., 2004). Similar conditions could also lead to the development of deep weathering profiles as observed along the Western Ghats (Beauvais et al., 2016). When compared with these contexts, it can be proposed that the high denudation rates observed across the SEAE correspond to a combination of a granitic lithology prone to weathering and a temperate climate with moderate mean annual precipitation and temperature that limits weathering profiles development such that they do not act as an inhibitor to landscape evolution. Despite a well developed saprolite (Green et al., 2006; Dosseto et al., 2008), measured soil thicknesses in the Bega valley are usually < 1 m (e.g. Heimsath et al., 2000) and instances of outcropping bedrock are common.

Many studies have investigated the relationship between denudation rates and climatic parameters (e.g. Portenga and Bierman, 2011). However, such comparisons are often complicated by the underlying variability in the morphological contexts of the sampling sites, in particular topographic gradients. We integrate this topographic effect by comparing the regression slopes of CWDR against average topographic gradient (Figure 5A) with the Mean

270 Annual Precipitation (MAP) from Hijmans et al. (2005) (Figure 5B). For shallow hillslopes, the regression slope of CWDR against topographic gradients can be used as a proxy for the efficiency of hillslope denudation and transport processes and covaries with hillslope diffusion coefficient (equation 3).

275 As discussed above, lithological control most likely accounts for the low regression slope value of the South-African escarpment dataset (Scharf et al., 2013), when compared to the higher sensitivity observed for the Namibian dataset where MAP is equivalent. For escarpments under wetter conditions in Brazil, Sri Lanka or India, a nearly 4-fold increase in MAP induces a less

280 than 2-fold change in sensitivity (Figure 5B). Notably, we observe that the sensitivity of denudation rates to hillslope gradients is almost equivalent in arid Namibia and wet Sri Lanka, despite the major contrast in climatic conditions experienced by these the escarpments. This lack of significant increase in the efficiency of hillslope denudation processes could again be attributed

285 to the combined effects of bedrock protection by thicker regoliths and stabilization of soils by denser vegetation. The sensitivity increases significantly only when the high MAP value characterizing the Western Ghats is reached. The dataset from the SEAE stands out in this comparison by exhibiting the highest sensitivity at an intermediate MAP value of ~ 1000 mm. Again, this

290 high efficiency of hillslope processes could be related to the limited extent of soil profiles, allowing bedrock to keep providing fresh material to a mobile regolith. It could correspond to an intermediate optimum situation between dry and wet extremes, where water availability is sufficient to activate surface processes without triggering inhibiting effects by deep weathering and dense vegetation. This result bears similarities with the classical observation

295 of Langbein and Schumm (1958) that sediment yields peak at intermediate MAP values, even though in our case the optimal MAP appear to be slightly higher and the variable of interest is the sensitivity of erosion processes to topographic gradients.

300 It should be noted that the discussion above relies only on one data point corresponding to the SEAE. In order to gain broader insights into the climatic sensitivity this analysis was expanded to other type of settings, beyond passive margin escarpments, using the OCTOPUS database (Codilean et al., 2018). We filtered this database by selecting only catchments with area between 5 and 500 km², average gradient below 0.5 and average elevation below

305 4000 m. Additionally, we retained only data from studies with at least 5 catchments matching these criteria for further processing. Linear regressions

of CWDR against topographic gradient were performed for each of these regional datasets to extract the regression slope. The regressions were forced through the origin and the analysis was limited to studies where $R^2 > 0.8$ and $p < 0.01$ (Figure 5B). When focusing on settings where denudation rates are comparable with passive margin escarpments (< 100 mm/ka), we observe a general trend similar to that described above. In particular, we note that most values in the intermediate 1000-2000 mm MAP range display sensitivities in excess of 100 mm/ka, similar or higher to what we observe along the Southeastern Australian Escarpment. Accordingly, we consider that the initially surprisingly high regression slope obtained from the SEAE data is not an outlier but is actually representative of landscape evolution and efficiency of hillslope processes in this range of climatic conditions. Settings where the average denudation is higher than 100 mm/ka display significantly higher sensitivity of denudation to topographic gradients. However, no clear dependency on MAP can be observed, which suggests that in those settings submitted to higher rock uplift rates, tectonics might exert an overriding control on surface processes with respect to climate.

The evolution of the sensitivity of denudation rates across various climatic regimes illustrates the complexity of the relationship between surface processes and precipitation (Langbein and Schumm, 1958; Schaller et al., 2018). Our results thus strengthen the assumption that precipitation does not simply activate surface processes by increasing runoff, but also promotes a number of complex feedbacks through weathering history of the substrate (von Blanckenburg et al., 2004) and development of vegetation (Torres Acosta et al., 2015; Olen et al., 2016).

5.2. Long wavelength transience and escarpment retreat rate

Different types of numerical models have been developed to explore the dynamics and mode of evolution of passive margin escarpments. Recently, Braun (2018) proposed a formalism allowing to quantify the rate of divide migration based on the values of the fluvial and hillslope erosion efficiency coefficients. The underlying idea is that a contrast in denudation rates from both sides of the divide should drive its displacement at a fixed rate controlled by the difference in slopes. Passive margin escarpments are special cases of very asymmetric divides, where the plateau side displays shallow slopes. In this context, taking into account hillslope and fluvial processes, Braun (2018)

showed that the divide migration rate v_d can be written as,

$$v_d = 2 (K_f k^m)^{\frac{1}{mp+1}} K_d^{\frac{mp}{mp+1}}, \quad (7)$$

where K_f and K_d are the fluvial incision efficiency coefficient and linear hill-
 345 slope diffusion coefficient, respectively. Other parameters are m , the area
 exponent of the stream power incision law, and p and k the parameters of
 Hack's law. Implementing this approach for the study of an escarpment
 requires to constrain the fluvial incision and hillslope denudation efficiency
 coefficients K_f and K_d . We can estimate the fluvial incision efficiency or
 350 erodibility coefficient using the expression for steepness index, $ks = \frac{E}{K_f}^{1/n}$,
 and setting the slope exponent of the stream power law $n = 1$. A linear fit
 through our dataset allows to constrain $K_f = 3.0 \pm 0.5 \cdot 10^{-7} \text{ m}^{0.1}/\text{a}$ (Figure
 4A). We note that this value is highly similar to independent estimates de-
 rived from late Cenozoic river incision in the Lachlan catchment, north of
 355 our study area (van der Beek and Bishop, 2003).

The hillslope diffusion coefficient K_d can be constrained from hilltop curva-
 ture C_{HT} (Figure 3) using equation 4. We do not have an estimation of the
 average C_{HT} for each of the basins in which CWDR have been determined,
 but average values for the lowlands and highlands can be used to provide
 360 constraints on K_d . In the lowlands, using a value of $C_{HT}=0.0068\pm 0.0030$
 m^{-1} , $E=16\pm 1 \text{ mm/ka}$ and $\beta=2$ yields $K_d=0.0046\pm 0.0020 \text{ m}^2/\text{a}$, which is
 similar to previous estimates in our study area (Heimsath et al., 2000; Green
 et al., 2006). In the highlands, where $C_{HT}=0.0042\pm 0.0028 \text{ m}^{-1}$ and $E=10\pm 3$
 mm/ka , we obtain an identical value of $K_d=0.0048\pm 0.0035 \text{ m}^2/\text{a}$.

Using equation 7, with typical values of $m=0.45$ for the area exponent of the
 365 fluvial incision law, and $p = 5/3$ and $k = 6.7 \text{ m}^{0.33}$ for Hack's law parameters
 (see Supplementary Materials), allows calculating a rate of divide migration
 in the 40-80 m/Ma range (Figure 6), with most of the variability being as-
 sociated with the uncertainties on our estimates of K_d .

As reviewed and discussed by Braun (2018), inferred escarpment retreat
 370 rates spread over an order of magnitude depending on the methodologies
 used : from slow rates deduced mostly from cosmogenic nuclides and low-
 temperature thermochronology data (10s of m/Ma) to much faster evolution
 proposed by some geological and numerical modeling studies (100s of m/Ma).
 375 In the case of the Bega valley, our values for escarpment retreat rates are com-
 parable with those inferred by Heimsath et al. (2006) using independent data
 at the same location, but significantly slower than the propositions from the

numerical models by Braun (2018), which illustrate situations where slow denudation rates in the vicinity of the escarpment are coincident with significantly higher rates of divide migration.

Nott et al. (1996) have highlighted the complex processes of escarpment evolution, showing that headward propagation of gorges cutting through the escarpment at rates of several km/Ma outpace other processes by at least one order of magnitude. The rates of retreat we present here are calculated based on long-wavelength estimates of erosion efficiency parameters for hillslope and fluvial processes and are slightly lower but comparable with the retreat rate of 170 m/Ma inferred for the major escarpment by Nott et al. (1996), suggesting that slow retreat of the long wavelength escarpment face might not be incompatible with faster localized down-cutting of individual gorges. The existence of such sustained differences in the rates of landscape evolution along the escarpment could locally promote the development of embayments associated with the main incising rivers and increase its sinuosity over the long-term.

We also note that the values of the erosion efficiency coefficients K_f and K_d we calibrated in this context are one order of magnitude lower than the lowest values used by Braun (2018) in his parametric exploration. We should consider the possibility that the value of these coefficients can have evolved with time, notably due to changes in the climatic boundary condition. The fluvial erodibility coefficient K_f we calculated is strikingly similar to a long-term (~ 20 Ma) estimate obtained by van der Beek and Bishop (2003) in an adjacent area along the escarpment. Such similarity argues against order of magnitude changes of this parameter over the late Cenozoic. We do not have similar long-term estimates for the hillslope diffusion coefficient K_d but, considering our value of K_f , a retreat rate of 1 km/Ma would require a value of K_d 3 orders of magnitude higher than that we determined (Figure 6). The data acquired in our study area support slow rates of evolution for the escarpment at the 10-100 ka timescales. However, dissection and drainage integration driven by localized incision could promote much faster evolution at other locations.

5.3. Hillslope dynamics and short-wavelength transience

The retreat rate of the escarpment can also be discussed on the basis of hillslope parameters, such as hillslope length, relief and hilltop curvature, extracted from our high resolution DEM (Figure 3). We note that all these parameters are nearly constant across the lowlands area, at the foot of the

415 escarpment. Theoretical models of hillslope profiles evolution suggest that,
depending on their length and the value of the diffusion coefficient, hills-
lope topographic properties can retain a memory of transient evolution for
extended periods of time, up to several Ma (e.g. Hurst et al., 2012; Mudd,
2017), and in any case over a longer time span than that integrated by the cos-
420 mogenic nuclides, which is in the 10-100 ka range in our case (table S1). The
diffusion coefficient we determined allows to estimate a hillslope adjustment
timescale of the order of 1 Ma (figure 7). If the escarpment recently prop-
agated across the lowlands, a topographic signature would still be observed
in our transect of hilltop curvature, due to this long adjustment timescale
425 (Hurst et al., 2012). Thus, this part of our dataset also supports a slowly
evolving escarpment over recent time periods.

Further insights on the transient landscape dynamics may be derived by com-
paring values of the non-dimensional relief R^* and erosion rate E^* calculated
from the measured hillslope properties, with the steady state relationship of
430 Equation 6 (Roering et al., 2007; Grieve et al., 2016). Lying below the the-
oretical steady state curve, our dataset suggests relaxing transient dynamics
of the hillslopes (Figure 8). Several hypotheses may be invoked to explain
this observation. A decrease in long-wavelength rock uplift, induced for ex-
ample by local changes in mantle dynamics (e.g. Salles et al., 2017) would
435 induce a relaxation of hillslopes with a decrease in relief and hilltop curva-
ture. However, the information concerning this eventual uplift rate change
should propagate from the base level as a bottom-up signal (Mudd, 2017)
and would induce a gradient of the geomorphic parameters, such as hilltop
curvature, from the coast toward the escarpment. The fact that such gradi-
440 ents are not evidenced and that the hillslopes of the highlands, on the other
side of the divide, are similarly out of equilibrium, rather suggests that this
transient dynamics results from a top-down forcing (Mudd, 2017), most likely
of climatic origin.

One major difficulty in relating environmental changes to their impact on
445 hillslope dynamics and morphology is that such perturbations can simul-
taneously trigger various types of antagonistic responses. For example, an
increase in precipitation would imply more surface runoff, which is likely to
increase downslope soil transport efficiency. On the other hand, it may lead
to significant changes in vegetation, with complex effects on regolith mobil-
450 ity. Similarly, a fundamental parameter controlling hillslopes dynamics is
their length, defined by the complex competition between fluvial and hills-
lope response times, which are both controlled by climate-dependent erosion

efficiency parameters (e.g. Perron et al., 2009).

The last deglaciation has triggered important environmental changes throughout Australia, including shifts in land cover, upheavals of sedimentary dynamics and an increase in effective precipitation (e.g. Ayliffe et al., 1998; Dosseto et al., 2010; Petherick et al., 2013). Important aggradation events have been shown to occur over the Late Pleistocene and Holocene in Southeastern Australia (e.g. Prosser et al., 1994). However, the proposed long hillslope adjustment time scales question the idea that such high-frequency perturbations, operating at the 10 ka timescale, could impact hillslope morphology to the extent observed here (Figure 7). Lower frequency climatic forcing acting over 100 ka to 1 Ma timescales associated, for example, with Late Cenozoic global cooling, would be more likely to lead to such a pronounced imprint, even though further investigation is required to elucidate the nature of this response.

In any case, our observations highlight the combination of two types of transient evolution in the present-day dynamics of the escarpment. Long-wavelength processes contribute to the slow and progressive inland retreat of this major topographic barrier over millions of years, while smaller-scale transient response of individual hillslopes is tuned to the higher frequency beat of climatic fluctuations.

6. Conclusion

Our study is one of the first to combine high-resolution topographic analysis and catchment-wide denudation rates calculated at the scale of an escarpment, from the lowlands up to the highlands. We also demonstrate the utility of Pléiades-derived Digital Elevation Models in process-oriented quantitative geomorphology studies. The acquired datasets allow us to investigate the dynamics of the South Eastern Australian Escarpment at different spatial scales. Our analysis illustrates a complex behavior combining long-term dynamics triggered by tectonic forcings and shorter-term climatic imprint. We also provide the first application to an actual field setting of the novel methodology proposed by Braun (2018) and compute a retreat rate of 40-80 mm/ka for the SE Australian Escarpment over the last 100 ka.

When compared with other similar geological and tectonic settings worldwide, our study area stands out with significantly higher denudation rates and dependency on hillslope topographic gradients, which we interpret as an effect of its temperate climate on weathering history and vegetation. This

observation is supported by global datasets suggesting that hillslope processes are most sensitive to topographic gradients in a narrow band of MAP
490 corresponding to 1000-1500 mm MAP.

While the transient response of landscape to external forcings is a well studied phenomenon, most analyses have focused on a particular spatial scale. In the studied area, we show that transience is present at various spatial
495 scales from the hillslope to the whole escarpment, as evidenced by the spatial distribution of morphological properties and denudation patterns. One key challenge in Geomorphology is to understand the relationships between different types of influences acting on landscapes, and in particular the potential feedbacks between top-down and bottom-up forcings (e.g. Mudd, 2017).
500 Interestingly, the two types of transience documented in our study have contrasted origins, such that bottom-up tectonic and top-down climatic influences are interwoven and result into a complex landscape dynamics. This observation highlights the importance of analyzing Earth-surface processes across wavelengths in order to understand how elementary processes operating at small-scale are integrated to contribute to the dynamics of relief over
505 10's of kilometers.

Acknowledgements

This research was supported by the Centre National d'études Spatiales (CNES) TOSCA program. The Pléiades images used in this study were
510 obtained through an ISIS project funded by the CNES. The French AMS national facility ASTER (CEREGE, Aix-en-Provence) is supported by the INSU/CNRS, ANR through the "Projets thmatique d'excellence" Program for the "Equipements d'Excellence" ASTER-CEREGE action, IRD, and CEA. We thank Arjun Heimsath and Peter van der Beek for insightful comments on the manuscript.
515

References

Ayliffe, L.K., Marianelli, P.C., Moriarty, K.C., Wells, R.T., McCulloch, M.T., Mortimer, G.E., Hellstrom, J.C., 1998. 500 ka precipitation record from southeastern Australia: Evidence for interglacial relative aridity. *Geology*
520 26, 147–150. doi:10.1130/0091-7613(1998)026<0147:KPRFSA>2.3.CO;2.

- Beauvais, A., Bonnet, N.J., Chardon, D., Arnaud, N., Jayananda, M., 2016. Very long-term stability of passive margin escarpment constrained by $^{40}\text{Ar}/^{39}\text{Ar}$ dating of K-Mn oxides. *Geology* 44, 299–302. doi:10.1130/G37303.1.
- 525
- van der Beek, P., Bishop, P., 2003. Cenozoic river profile development in the Upper Lachlan catchment (SE Australia) as a test of quantitative fluvial incision models. *Journal of Geophysical Research: Solid Earth* 108. URL: <http://doi.wiley.com/10.1029/2002JB002125>, doi:10.1029/2002JB002125.
- 530
- van der Beek, P., Braun, J., 1998. Numerical modelling of landscape evolution on geological time- scales: A parameter analysis and comparison with the south- eastern highlands of Australia. *Basin Research* 10, 49–68. doi:10.1046/j.1365-2117.1998.00056.x.
- 535
- Beeson, H.W., McCoy, S.W., Keen-Zebert, A., 2017. Geometric disequilibrium of river basins produces long-lived transient landscapes. *Earth and Planetary Science Letters* 475, 34–43. URL: <http://dx.doi.org/10.1016/j.epsl.2017.07.010><http://linkinghub.elsevier.com/retrieve/pii/S0012821X17303886>, doi:10.1016/j.epsl.2017.07.010.
- 540
- Bierman, P.R., Caffee, M., 2001. Slow rates of rock surface erosion and sediment production across the Namib Desert and escarpment, Southern Africa. *American Journal of Science* 301, 326–358. doi:10.2475/ajs.301.4-5.326.
- 545
- von Blanckenburg, F., Hewawasam, T., Kubil, P.W., 2004. Cosmogenic nuclide evidence for low weathering and denudation in the wet, tropical highlands of Sri Lanka. *Journal of Geophysical Research* 109, F03008. URL: <http://doi.wiley.com/10.1029/2003JF000049>, doi:10.1029/2003JF000049.
- 550
- Braun, J., 2018. A review of numerical modeling studies of passive margin escarpments leading to a new analytical expression for the rate of escarpment migration velocity. *Gondwana Research* 53, 209–224. URL: <http://linkinghub.elsevier.com/retrieve/pii/S1342937X17302058>, doi:10.1016/j.gr.2017.04.012.

- 555 Braun, J., van der Beek, P.A., 2004. Evolution of passive margin escarpments: What can we learn from low-temperature thermochronology? *Journal of Geophysical Research* 109, F04009. URL: <http://www.agu.org/pubs/crossref/2004/2004JF000147.shtml>, doi:10.1029/2004JF000147.
- 560 Cherem, L.F.S., Varajão, C.A.C., Braucher, R., Bourlés, D., Salgado, A.A.R., Varajão, A.C., 2012. Long-term evolution of denudational escarpments in southeastern Brazil. *Geomorphology* 173-174, 118–127. URL: <http://dx.doi.org/10.1016/j.geomorph.2012.06.002>, doi:10.1016/j.geomorph.2012.06.002.
- 565 Cockburn, H., Brown, R., Summerfield, M., Seidl, M., 2000. Quantifying passive margin denudation and landscape development using a combined fission-track thermochronology and cosmogenic isotope analysis approach. *Earth and Planetary Science Letters* 179, 429–435. URL: [http://dx.doi.org/10.1016/S0012-821X\(00\)00144-8](http://dx.doi.org/10.1016/S0012-821X(00)00144-8), doi:10.1016/S0012-821X(00)00144-8.
- 570 Codilean, A.T., Bishop, P., Stuart, F.M., Hoey, T.B., Fabel, D., Freeman, S.P., 2008. Single-grain cosmogenic ²¹Ne concentrations in fluvial sediments reveal spatially variable erosion rates. *Geology* 36, 159. URL: <http://geology.gsapubs.org/content/36/2/159.short>, doi:10.1130/G24360A.1.
- 575 Codilean, A.T., Munack, H., Cohen, T.J., Saktura, W.M., Gray, A., Mudd, S.M., 2018. OCTOPUS: An Open Cosmogenic Isotope and Luminescence Database. *Earth System Science Data Discussions* , 1–23 URL: <https://www.earth-syst-sci-data-discuss.net/essd-2018-32/>, doi:10.5194/essd-2018-32.
- 580 Czarnota, K., Roberts, G.G., White, N.J., Fishwick, S., 2014. Spatial and temporal patterns of Australian dynamic topography from River Profile Modeling. *Journal of Geophysical Research: Solid Earth* 119, 1384–1424. URL: <http://doi.wiley.com/10.1002/2013JB010436>, doi:10.1002/2013JB010436.
- 585 Dosseto, A., Buss, H.L., Chabaux, F., 2014. Age and weathering rate of sediments in small catchments: The role of hillslope erosion. *Geochimica et Cosmochimica Acta* 132, 238–258. URL: <http://linkinghub>.

elsevier.com/retrieve/pii/S0016703714000982, doi:10.1016/j.gca.2014.02.010.

590 Dosseto, A., Hesse, P.P., Maher, K., Fryirs, K., Turner, S., 2010. Climatic and vegetation control on sediment dynamics during the last glacial cycle. *Geology* 38, 395–398. URL: <http://geology.geoscienceworld.org/content/38/5/395.full>, doi:10.1130/G30708.1.

Dosseto, A., Turner, S.P., Chappell, J., 2008. The evolution of weathering profiles through time: New insights from uranium-series isotopes. *Earth and Planetary Science Letters* 274, 359–371. doi:10.1016/j.epsl.2008.07.050.

Fox, M., Goren, L., May, D.A., Willett, S.D., 2014. Inversion of fluvial channels for paleorock uplift rates in Taiwan. *Journal of Geophysical Research: Earth Surface* 119, 1853–1875. URL: <http://doi.wiley.com/10.1002/2014JF003196>, doi:10.1002/2014JF003196.

Green, E.G., Dietrich, W.E., Banfield, J.F., 2006. Quantification of chemical weathering rates across an actively eroding hillslope. *Earth and Planetary Science Letters* 242, 155–169. doi:10.1016/j.epsl.2005.11.039.

605 Grieve, S.W.D., Mudd, S.M., Hurst, M.D., Milodowski, D.T., 2016. A non-dimensional framework for exploring the relief structure of landscapes. *Earth Surface Dynamics* 4, 309–325. doi:10.5194/esurf-4-309-2016.

Heimsath, A.M., Chappell, J., Dietrich, W.E., Nishiizumi, K., Finkel, R.C., 2000. Soil production on a retreating escarpment in southeastern Australia. *Geology* 28, 787–790. URL: <http://geology.gsapubs.org/content/28/9/787.short>, doi:10.1130/0091-7613(2000)28.

Heimsath, A.M., Chappell, J., Dietrich, W.E., Nishiizumi, K., Finkel, R.C., 2001. Late Quaternary erosion in southeastern Australia: a field example using cosmogenic nuclides. *Quaternary International* 83-85, 169–185. URL: [http://dx.doi.org/10.1016/S1040-6182\(01\)00038-6](http://dx.doi.org/10.1016/S1040-6182(01)00038-6), doi:10.1016/S1040-6182(01)00038-6.

Heimsath, A.M., Chappell, J., Fifield, K., 2010. *Eroding Australia: rates and processes from Bega Valley to Arnhem Land*. Geological Society, London, Special Publications 346, 225–241. doi:10.1144/SP346.12.

- 620 Heimsath, A.M., Chappell, J., Finkel, R.C., Fifield, K., Alimanovic,
A., 2006. Escarpment erosion and landscape evolution in south-
eastern Australia, in: Special Paper 398: Tectonics, Climate, and
Landscape Evolution. Geological Society of America. volume 398, pp.
173–190. URL: [http://books.google.com/books?hl=en&lr=&id=-Zg0Y8ftvjwC&oi=fnd&pg=PA173&dq=Escarpment+erosion+and+landscape+evolution+in+southeastern+Australia&ots=gXNkXJQ\[_\]6R&sig=ISHet6FUo7EyKjMZyEy47L0X8k{ }5Cnhttp://books.google.com/books?hl=](http://books.google.com/books?hl=en&lr=&id=-Zg0Y8ftvjwC&oi=fnd&pg=PA173&dq=Escarpment+erosion+and+landscape+evolution+in+southeastern+Australia&ots=gXNkXJQ[_]6R&sig=ISHet6FUo7EyKjMZyEy47L0X8k{ }5Cnhttp://books.google.com/books?hl=), doi:10.1130/2006.2398(10).
- Heimsath, A.M., Chappell, J., Spooner, N.A., Questiaux, D.G., 2002. Creep-
630 ing soil. *Geology* 30, 111–114. doi:10.1130/0091-7613(2002)030<0111:
CS>2.0.CO.
- Hijmans, R.J., Cameron, S.E., Parra, J.L., Jones, P.G., Jarvis, A., 2005.
Very high resolution interpolated climate surfaces for global land areas.
International Journal of Climatology 25, 1965–1978. doi:10.1002/joc.
635 1276.
- Hurst, M.D., Mudd, S.M., Attal, M., Hilley, G., 2013. Hillslopes record the
growth and decay of landscapes. *Science* 341, 868–871. URL: <http://www.sciencemag.org/content/341/6148/868.short>, doi:10.1126/science.
1241791.
- 640 Hurst, M.D., Mudd, S.M., Walcott, R., Attal, M., Yoo, K., 2012. Using
hilltop curvature to derive the spatial distribution of erosion rates. *Journal
of Geophysical Research* 117, F02017. URL: [http://www.agu.org/pubs/
crossref/2012/2011JF002057.shtml](http://www.agu.org/pubs/crossref/2012/2011JF002057.shtml), doi:10.1029/2011JF002057.
- Langbein, W.B., Schumm, S.A., 1958. Yield of sediment in relation to mean
645 annual precipitation. *Transactions, American Geophysical Union* 39, 1076.
URL: <http://doi.wiley.com/10.1029/TR039i006p01076>, doi:10.1029/
TR039i006p01076.
- Mandal, S.K., Lupker, M., Burg, J.P., Valla, P.G., Haghypour, N., Christl,
M., 2015. Spatial variability of ¹⁰Be-derived erosion rates across
650 the southern Peninsular Indian escarpment: A key to landscape evo-
lution across passive margins. *Earth and Planetary Science Letters*
425, 154–167. URL: [http://linkinghub.elsevier.com/retrieve/pii/
S0012821X15003489](http://linkinghub.elsevier.com/retrieve/pii/S0012821X15003489), doi:10.1016/j.epsl.2015.05.050.

- 655 Matmon, A., Bierman, P., Enzel, Y., 2002. Pattern and tempo of great escarpment erosion. *Geology* 30, 1135–1138. URL: <http://geology.geoscienceworld.org/content/30/12/1135.full>, doi:10.1130/0091-7613(2002)030<1135:PAT0GE>2.0.CO;2.
- Mudd, S.M., 2017. Detection of transience in eroding landscapes. *Earth Surface Processes and Landforms* 42, 24–41. URL: <http://doi.wiley.com/10.1002/esp.3923>, doi:10.1002/esp.3923.
- 660 Nott, J., Young, R., McDougall, I., 1996. Wearing Down, Wearing Back, and Gorge Extension in the Long-Term Denudation of a Highland Mass: Quantitative Evidence from the Shoalhaven Catchment, Southeast Australia. *The Journal of Geology* 104, 224–232.
- 665 Olen, S.M., Bookhagen, B., Strecker, M.R., 2016. Role of climate and vegetation density in modulating denudation rates in the Himalaya. *Earth and Planetary Science Letters* 445, 57–67. URL: <http://dx.doi.org/10.1016/j.epsl.2016.03.047>, doi:10.1016/j.epsl.2016.03.047.
- Perron, J.T., Kirchner, J.W., Dietrich, W.E., 2009. Formation of evenly spaced ridges and valleys. *Nature* 460, 502–505. URL: <http://dx.doi.org/10.1038/nature08174>, doi:10.1038/nature08174.
- 670 Persano, C., Stuart, F.M., Bishop, P., Barfod, D.N., 2002. Apatite (UTh)/He age constraints on the development of the Great Escarpment on the southeastern Australian passive margin. *Earth and Planetary Science Letters* 200, 79–90. URL: [http://dx.doi.org/10.1016/S0012-821X\(02\)00614-3](http://dx.doi.org/10.1016/S0012-821X(02)00614-3), doi:10.1016/S0012-821X(02)00614-3.
- 680 Petherick, L., Bostock, H., Cohen, T., Fitzsimmons, K., Tibby, J., Fletcher, M.S., Moss, P., Reeves, J., Mooney, S., Barrows, T., Kemp, J., Jansen, J., Nanson, G., Dosseto, A., 2013. Climatic records over the past 30 ka from temperate Australia a synthesis from the Oz-INTIMATE workgroup. *Quaternary Science Reviews* 74, 58–77. URL: <http://dx.doi.org/10.1016/j.quascirev.2012.12.012><http://linkinghub.elsevier.com/retrieve/pii/S0277379112005409>, doi:10.1016/j.quascirev.2012.12.012.
- 685 Portenga, E.W., Bierman, P.R., 2011. Understanding Earth’s eroding surface with 10Be. *GSA Today* 21, 44–10. URL: <http://www.geosociety.org/gsatoday/archive/21/8/article/i1052-5173-21-8-4.htm>.

- Portenga, E.W., Rood, D.H., Bishop, P., Bierman, P.R., 2016. A late
Holocene onset of Aboriginal burning in southeastern Australia. *Geol-
690 ogy* 44, 131–134. URL: <http://geology.gsapubs.org/lookup/doi/10.1130/G37257.1>, doi:10.1130/G37257.1.
- Prosser, I.P., Chappell, J., Gillespie, R., 1994. Holocene valley aggra-
dation and gully erosion in headwater catchments, south-eastern high-
lands of Australia. *Earth Surface Processes and Landforms* 19, 465–480.
695 URL: <http://doi.wiley.com/10.1002/esp.3290190507>, doi:10.1002/
esp.3290190507.
- Roering, J.J., Kirchner, J.W., Dietrich, W.E., 2001. Hillslope evolution
by nonlinear, slope-dependent transport: Steady state morphology and
equilibrium adjustment timescales. *Journal of Geophysical Research* 106,
700 16499–16513. doi:10.1029/2001JB9000323.
- Roering, J.J., Perron, J.T., Kirchner, J.W., 2007. Functional relationships
between denudation and hillslope form and relief. *Earth and Planetary Sci-
ence Letters* 264, 245–258. URL: <http://dx.doi.org/10.1016/j.epsl.2007.09.035>.
- 705 Salgado, A.A.R., Marent, B.R., Cherem, L.F.S., Bourlès, D., Santos, L.J.C.,
Braucher, R., Barreto, H.N., 2014. Denudation and retreat of the Serra do
Mar escarpment in southern Brazil derived from in situ-produced ^{10}Be
concentration in river sediment. *Earth Surface Processes and Landforms*
39, 311–319. URL: <http://doi.wiley.com/10.1002/esp.3448>, doi:10.
710 1002/esp.3448.
- Salgado, A.A.R., Rezende, E.d.A., Bourlès, D., Braucher, R., da Silva, J.R.,
Garcia, R.A., 2016. Relief evolution of the Continental Rift of South-
east Brazil revealed by in situ-produced ^{10}Be concentrations in river-
borne sediments. *Journal of South American Earth Sciences* 67, 89–99.
715 doi:10.1016/j.jsames.2016.02.002.
- Salles, T., Flament, N., Müller, D., 2017. Influence of man-
tle flow on the drainage of eastern Australia since the Juras-
sic Period. *Geochemistry, Geophysics, Geosystems* 15, 4424–
4444. URL: <http://doi.wiley.com/10.1002/2014GC005506>
720 <http://doi.wiley.com/10.1002/2016GC006617>, doi:10.1002/2016GC006617,
arXiv:arXiv:1605.08479.

- Schaller, M., Ehlers, T., Lang, K., Schmid, M., Fuentes-Espoz, J., 2018. Addressing the contribution of climate and vegetation cover on hillslope denudation, Chilean Coastal Cordillera (26-38S). *Earth and Planetary Science Letters* 489, 111–122. URL: <http://linkinghub.elsevier.com/retrieve/pii/S0012821X18300888>, doi:10.1016/j.epsl.2018.02.026.
- 725
- Scharf, T.E., Codilean, A.T., de Wit, M., Jansen, J.D., Kubik, P.W., 2013. Strong rocks sustain ancient postorogenic topography in southern Africa. *Geology* 41, 331–334. URL: <http://geology.gsapubs.org/content/41/3/331.short>, doi:10.1130/G33806.1.
- 730
- Torres Acosta, V., Schildgen, T.F., Clarke, B.A., Scherler, D., Bookhagen, B., Wittmann, H., von Blanckenburg, F., Strecker, M.R., 2015. Effect of vegetation cover on millennial-scale landscape denudation rates in East Africa. *Lithosphere* 7, 408–420. URL: <https://pubs.geoscienceworld.org/lithosphere/article/7/4/408-420/145743>, doi:10.1130/L402.1.
- 735
- Tucker, G.E., Whipple, K.X., 2002. Topographic outcomes predicted by stream erosion models: Sensitivity analysis and intermodel comparison. *Journal of Geophysical Research* 107, 2179. URL: <http://www.agu.org/pubs/crossref/2002/2001JB000162.shtml>.
- 740
- Weissel, J.K., Seidl, M.A., 1997. Influence of rock strength properties on escarpment retreat across passive continental margins. *Geology* 25, 631–634. URL: <http://geology.geoscienceworld.org/content/25/7/631.abstract>, doi:10.1130/0091-7613(1997)025<0631:IORSP0>2.3.CO;2.

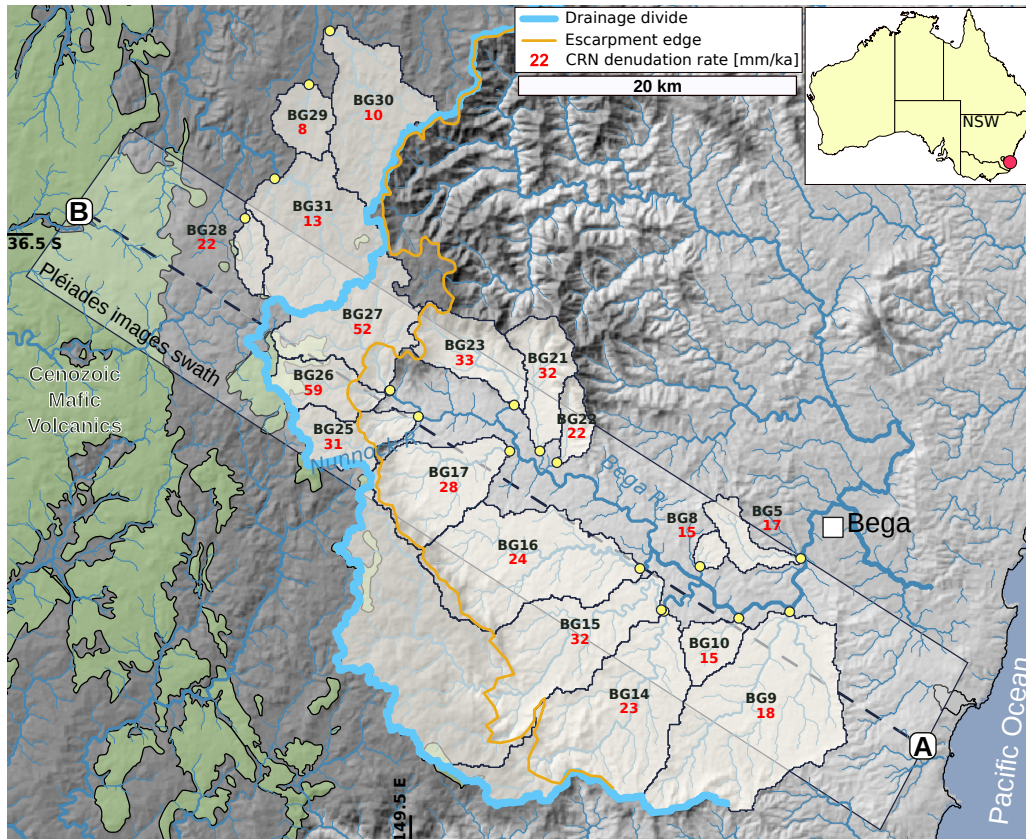


Figure 1: Shaded relief map of the studied area (ASTER GDEM). Light blue and orange lines indicate the positions of the drainage divide and lip of the escarpment, respectively. Yellow circles are sampling locations of river sands used in detrital cosmogenic analyses, shaded areas are the catchments boundaries and red numbers indicate the calculated denudation rates in mm/ka.

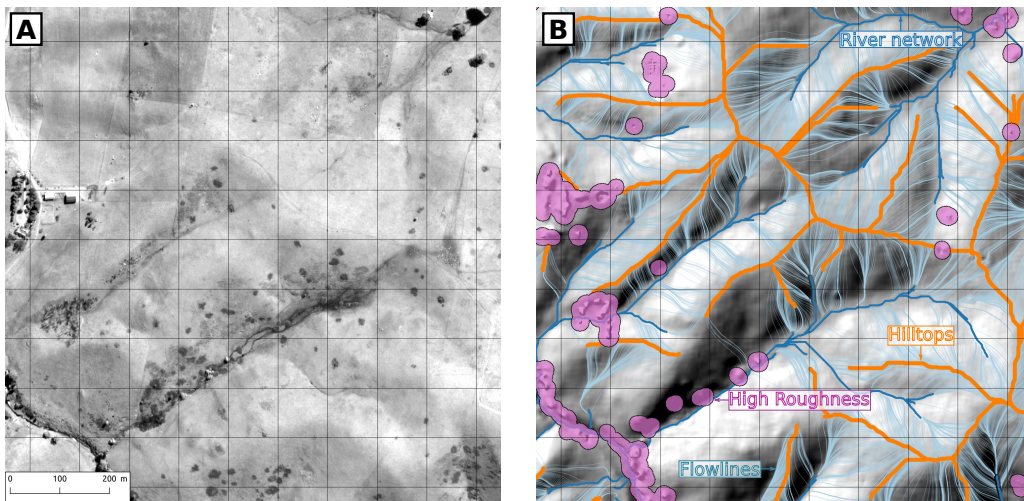


Figure 2: A - Orthorectified Pléiades image of a selected sector in the lowlands. B - Corresponding shaded Digital Elevation Model displaying the main landscape features used in the morphometric analysis. Dark blue lines : river network. Purple areas : high Topographic Roughness Index (TRI) areas excluded from the analysis. Orange lines : hilltops. Light blue thin lines : flowlines routed from the hilltops down to the river network. See supplementary materials for details of the processing.

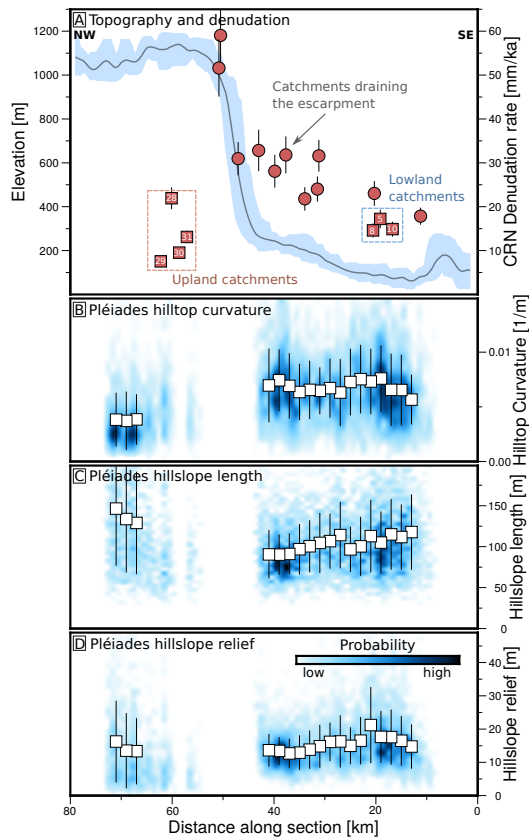


Figure 3: A - Topographic cross-section across the escarpment (see figure 1 for location). Squares indicate the denudation rates of catchments draining exclusively the lowlands or highlands, whereas circles correspond to catchments draining across the escarpment. Position of data points corresponds to the catchments centroids. B - Hilltop curvature extracted from Pléiades 1 m DEM. White squares are the average values calculated along 2 km wide bins, with vertical bars corresponding to $\pm 1\sigma$. C - Hillslope length extracted from Pléiades 1 m DEM. D - Hillslope relief extracted from Pléiades 1 m DEM.

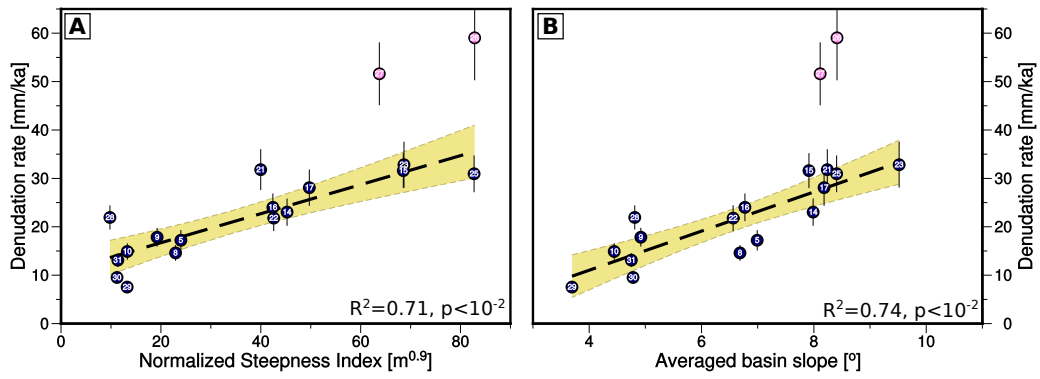


Figure 4: A - CRN denudation rates as a function of normalized steepness index for the studied catchments. Numbers refer to samples names. The black dashed line is a linear fit through the data and the yellow area is the 95% confidence envelope. Pink symbols are catchments BG26 and BG27 that have been excluded from the analysis, see text for further details. B - CRN denudation rates as a function of averaged slope for the studied catchments.

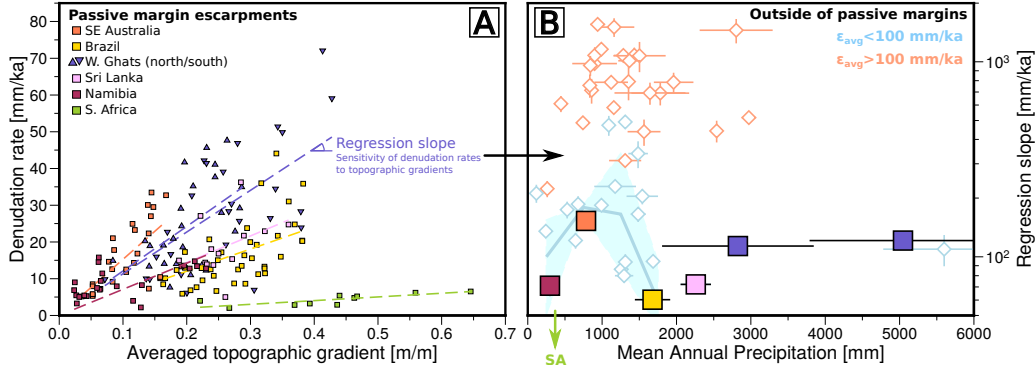


Figure 5: A - Relationships between denudation rate and average topographic gradient for selected studies on passive margin escarpments. These studies cover various climatic settings such as the South-Eastern Australian Escarpment (this study, Portenga et al., 2016), the Serra do Mar in Eastern Brazil (Cherem et al., 2012; Salgado et al., 2016), the Western Ghats of India (Mandal et al., 2015), Sri Lanka (von Blanckenburg et al., 2004) and the Namibian and South-African escarpments (Bierman and Caffee, 2001; Codilean et al., 2008; Scharf et al., 2013). Dashed lines are linear regression forced through the origin for the individual datasets. We subset the Western Ghats dataset into a southern and a northern part (limit at latitude 12°N) to account for the strong gradient in precipitation along the escarpment (Mandal et al., 2015). B - Regression slope of the Catchment Wide Denudation Rate against topographic gradient linear fit (sensitivity) as a function of Mean Annual Precipitation. Large squares correspond to the passive margin settings from inset A. The very low regression slope of the South African (SA) escarpment (10.1 mm/ka, MAP : 390 mm) is out of range for this plot. Diamonds correspond to additional regional studies outside of passive margin escarpments settings compiled in the OCTOPUS database (Codilean et al., 2018) and color-coded according to their average denudation rates (blue : <100 mm/ka). See text for additional information on data processing and selection. Blue curve and light blue envelope represent the median and interquartile range over 500 mm MAP intervals, for low denudation settings (<100 mm/ka). The curves are not extended beyond 2000 mm MAP due to the scarcity of data above this value.

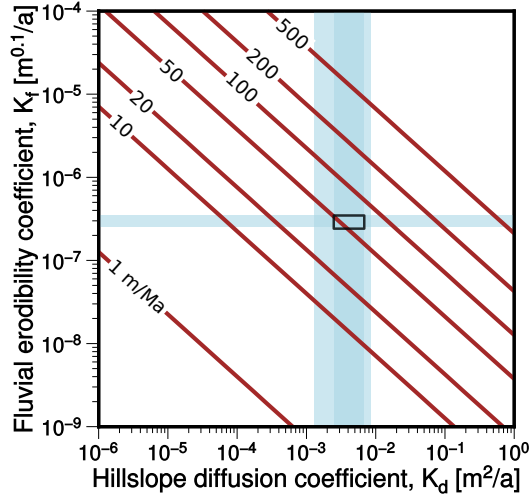


Figure 6: Retreat rates (dark red lines) as a function of the erosion efficiency coefficients K_d and K_f computed using equation 7 (Braun, 2018). Blue rectangles indicate the estimated ranges for these coefficients based on our dataset, including both highlands and lowlands estimates for K_d . Black rectangle indicates the overlapping ranges of the coefficients. See text for detail of the calculation and associated parameters.

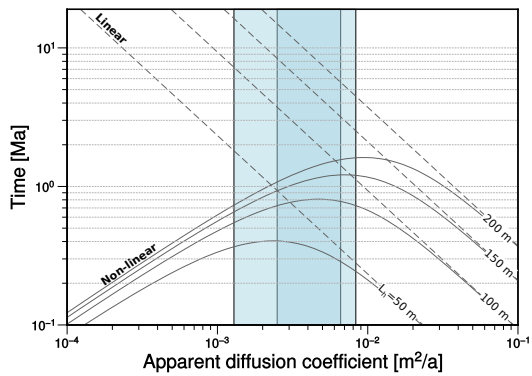


Figure 7: Adjustment time-scales of hillslopes based on linear (dashed lines) and non-linear (solid lines) evolution models (Roering et al., 2001; Hurst et al., 2012), for different values of the hillslope length L_h , and an erosion rate of 15 mm/ka. Blue shading correspond to the estimated values of the diffusion coefficient K_d for the lowlands and highlands.

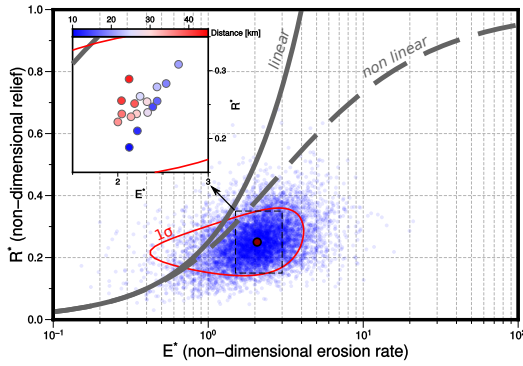


Figure 8: Non-dimensional relief (R^*) versus non-dimensional erosion rate (E^*) diagram for the hillslopes extracted from the high resolution Pléiades DEM. Solid grey line correspond to the steady state relationship between R^* and E^* when sediment flux is considered to be linear (Equation 6). Dashed grey line is the equivalent relationship in the non-linear case (e.g. Roering et al., 2007; Grieve et al., 2016). Critical hillslope gradient S_c is 0.6. Each blue dot represents a hilltop patch corresponding to at least 50 pixels. The dashed black box corresponds to the focus inset, where the data is binned according to the distance across the escarpment lowlands, using the same horizontal distance coordinates as Figure 3.